International Journal of Innovative
Computing, Information and Control
Volume **14**, Number **5**, October **2018**

 ISSN 1349-4198
pp. **1787–1804**

THE PERFORMANCE OF ADAPTIVE TUNING PIECEWISE CUBIC HERMITE INTERPOLATION MODEL FOR SIGNAL-TO-NOISE RATIO ESTIMATION

Kok Swee Sim, Zhi Xuan Yeap, Fung Fung Ting and Chih Ping Tso

Faculty of Engineering and Technology
Multimedia University
Jalan Ayer Keroh Lama, Bukit Beruang 75450, Melaka, Malaysia
{ kssim; cptso }@mmu.edu.my; zhixuanyeap@hotmail.com; sicily.ting@gmail.com

Received October 2017; revised February 2018

Abstract. *A technique based on the piecewise cubic Hermite interpolation (PCHI) model was previously applied to calculating the signal-to-noise ratio (SNR) in scanning electron microscope (SEM) images. An algorithm was also used by cascading the tuning technique, named adaptive tuning piecewise cubic Hermite interpolation (ATPCHIP) model. Comparisons were made with the performance of the other methods – adaptive slope nearest neighbourhood (ASNN), linear least square regression (LLSR) and nonlinear least square regression (NLLSR) through Cramer-Rao lower bound (CRLB), t-test, scatter plot and Bland-Altman plot. Using different images, the ATPCHIP single-image model is shown to be much better than other models.*
Keywords: Piecewise cubic Hermite interpolation, Signal-to-noise ratio, Scanning electron microscope images, Image processing

1. **Introduction.** Signal-to-noise ratio (SNR) is often used to judge the quality of images, since the amount of noise in an image affects the image clarity. Then, as a parameter, it is also of importance to provide adaptive averaging. Secondly, SNR can measure image quality of both on-line and off-line images.

The cross-correlation technique was presented in [1] for the direction of arrival (DOA) estimation. The cross-correlation was applied in [2] to evaluating SNR using digital image averaging. It is employed to calculate the resolution and the SNR of CD-SEMs, SNR evaluation on magnetic resonance imaging (MRI) in [3,4]. The main drawback of cross relation technique is that two images are required and they need to be aligned well. Cross-correlation also cannot be used to find the SNR of an extant image like a micrograph or a stored image. In [5], it was suggested to estimate SNR using a single image, but the accuracy was poor. A method using the statistical autoregressive model was proposed to estimate the power of noise-free image [6,32].

Although the performances of various SNR estimation techniques have been discussed [1,5-9], it is still difficult to compare the relative performance of these estimators since the performance metrics are not standardized. To make a proper comparison, the authors propose using the Cramer-Rao inequality. The Cramer-Rao lower bound (CRLB) is a well-known limit for the variance of any unbiased estimator [10-17]. The derivation of an approximate Cramer-Rao lower bound (CRLB) for the parameters of a multicomponent linear frequency modulated continuous wave (LFMCW) signal had been discussed in [15]. In real additive white Gaussian noise (AWGN), [18] has applied the mean square error (MSE) to measuring the performance. CRLB is derived for the estimation of SNR of

DOI: 10.24507/ijicic.14.05.1787

binary phase-shift keying (BPSK) and quaternary phase-shift keying (QPSK) modulated signal. The SNR asymptotic of CRLB was applied to estimating the SNR of binary phase shift keying modulated signals [19]. The fundamental performance limits for image registration were derived using Cramer-Rao bound [20]. In recent years, CRLB has been applied to passive radar system that employed signals as illuminators for target detection, tracking and estimation [10,11,21,22].

In this paper, an SNR estimation algorithm, ATPCHIP, has been proposed to recover the variance of additively corrupted zero mean noise. The estimation of SNR is computed through ATPCHIP for a single image. The main contribution is to quantify the bounds single image SNR estimation through the presented ATPCHIP. In addition, CRLB, t-test, scatter plot, and Bland-Altman plot are applied to testing the performance of the single image SNR estimator.

2. **Formation of the Problem.** Using earlier notations [6,20] $w(i,j) = s(i,j) + n(i,j)$ represents the sum of a corrupted image with an additive white noise, where $s(i,j)$ is the noise-free image and $n(i,j)$ is the additive noise, and an example is as shown in Figure 1. The two-dimensional autocorrelation function $\phi(i,j)$ with offset along the x-direction $\phi(i)$ at zero j offset is depicted in Figure 2.

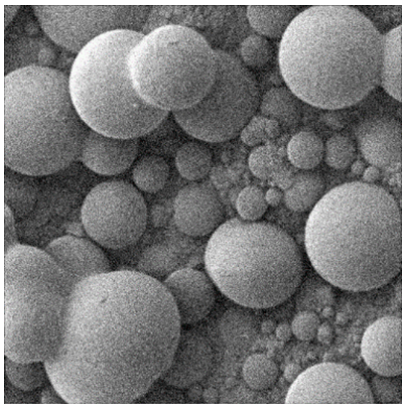

FIGURE 1. Power IC captured at beam diameter 151nm, with noise

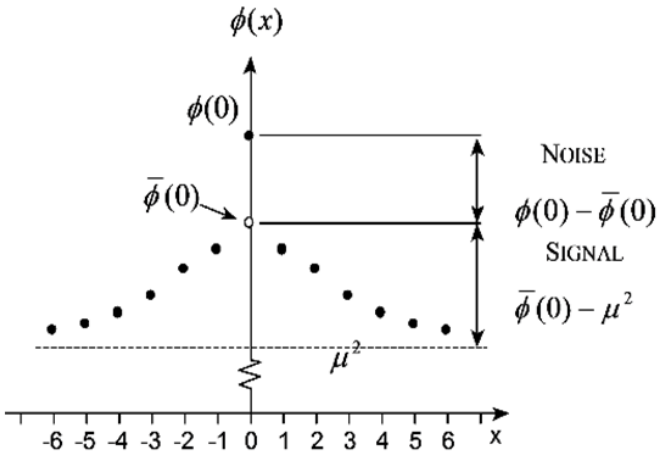

FIGURE 2. Representation of signal and noise components on a plot of the autocorrelation function, with the filled markers representing the data derived from the image

As $n(i,j)$ is considered as white and stationary along axis j, the SNR of a power IC captured at beam diameter = 151nm with noise can be obtained from the autocorrelation curve as shown in Figure 2.

It is clear in Figure 2 that $\phi(0) - \overline{\phi}(0)$ and $\overline{\phi}(0) - \mu^2$ represent the energies of the white noise and the energy of image signal, respectively, where μ is the image mean value. Then, the SNR is as in (1)

$$SNR = \frac{\overline{\phi}(0) - \mu^2}{\phi(0) - \overline{\phi}(0)} \tag{1}$$

To estimate the zero-offset autocorrelation point $\overline{\phi}(0)$ from an autocorrelation sequence, several single image SNR estimation techniques with different magnifications are corrupted with various noise levels and discussed below.

3. **The SNR Estimators.** The bias from the 4 methods, adaptive slope nearest neighbourhood (ASNN), linear least square regression (LLSR), non-linear least square regression (NLLSR) and adaptive tuning piecewise cubic Hermite interpolation (ATPCHIP), are computed for a collection of single images.

3.1. **Adaptive slope nearest neighbourhood.** This method was proposed by [7]. It is called as adaptive slope nearest neighbourhood (ASNN). It is an enhanced version of the existing nearest-neighbourhood method [5]. ASNN calculates the relation of $\overline{\phi}(0)$ through nearest-neighbourhood and noisy image zero-offset point $\phi(0)$. Then based on 100 images, 10 relationship graphs which are NV = 0.001 to 0.01 with increment 0.001 are plotted respectively. From the observation of graphs, when NV is increased, the SNR estimated using nearest-neighbourhood becomes more accurate and $\overline{\phi}(0)$ is always smaller than $\phi(0)$. The trend line is defined using $y = Sx + C$, and Figure 3 shows the linear trend line of estimated noise-free peak $\overline{\phi}(0)$ versus noisy peak $\phi(0)$ [7].

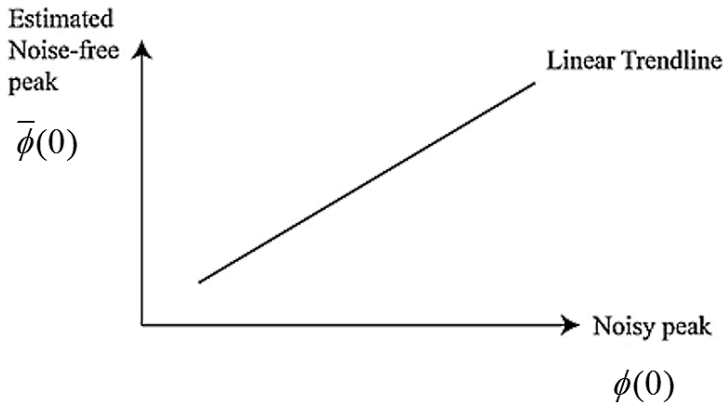

FIGURE 3. Linear trend line of estimated noise-free peak $\overline{\phi}(0)$ versus noisy peak $\phi(0)$

The method is implemented with Equation (2).

$$SNR_{predict} = (S) \times SNR_{actual} - C \tag{2}$$

where S is the slope of the trend line and C is the y-axis intercept.

3.2. **Linear least square regression.** [8] proposed a technique called the linear least square regression. The nearest neighbourhood point always has value lower than the peak and the noisy peak is always higher than the noise-free peak. Therefore, there is

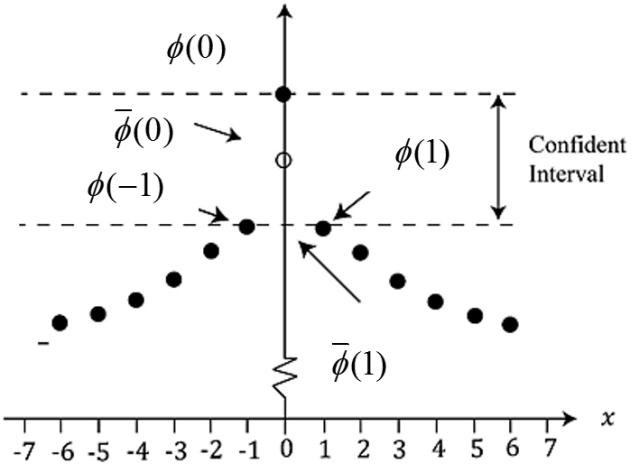

FIGURE 4. The confident interval of estimation in ACF curve

a confident interval between noisy peak and the nearest neighbourhood point. If any estimation result falls outside the confident interval, the value is void. Figure 4 shows the confident interval on the autocorrelation function (ACF) curve.

In this method, a line to best fit the data is determined. Equation (3) shows the linear least square regression equation [21,22].

$$\hat{y} = \alpha + x\beta \tag{3}$$

The prediction is started using Equation (3) by calculating the α and β. e is defined as the random error of $\hat{Y}$. After considering the e, Equation (3) can be written as

$$\hat{y} = \alpha + x\beta + e \tag{4}$$

In matrix form, it is

$$\hat{Y} = XB + \varepsilon \tag{5}$$

where

$$X = \begin{bmatrix} 1 & x_1 \\ 1 & x_{N+1} \\ \vdots & \vdots \\ 1 & x_N \end{bmatrix}, \quad e = \begin{bmatrix} e_1 \\ e_{N+1} \\ \vdots \\ e_N \end{bmatrix}, \quad \hat{Y} = \begin{bmatrix} y_1 \\ y_{N+1} \\ \vdots \\ y_N \end{bmatrix}, \quad B = \begin{bmatrix} \alpha \\ \beta \end{bmatrix}$$

X, e and Y are substituted into Equation (5) to get Equation (6).

$$\begin{bmatrix} y_1 \\ y_{N+1} \\ \vdots \\ y_N \end{bmatrix} = \begin{bmatrix} 1 & x_1 \\ 1 & x_{N+1} \\ \vdots & \vdots \\ 1 & x_N \end{bmatrix} \begin{bmatrix} \alpha \\ \beta \end{bmatrix} + \begin{bmatrix} e_1 \\ e_{N+1} \\ \vdots \\ e_N \end{bmatrix} \tag{6}$$

In order to get accurate estimation, e is assumed to be a value equal to half of the difference between the noisy peak and the nearest neighbourhood point. Equation of e is shown in Equation (7). After e is calculated, all the required values have been obtained, and the $\hat{y}$ can be acquired using Equation (8) [8].

$$e = \frac{\phi(0) - \phi(1)}{2} \tag{7}$$

$$\overline{\phi}(0) = \hat{y} = \alpha + x\beta + e \tag{8}$$

3.3. **Non-linear least square regression.** [9] also proposed a technique which is called non-linear least square regression. The first and second quadrants of the ACF curve show exponential growth. Figure 5 shows the exponential increment of the ACF curve.

Therefore, the idea of non-linear is to introduce the linear least square regression method.

Equation (8) is modified into non-linear form to fit the exponential characteristic of the ACF as in Figure 5.

$$\overline{\phi}(0) = \ln(\hat{y}) = \ln(\alpha) + x\beta + \ln(e) \tag{9}$$

Equation (9) can be simplified into Equation (10).

$$\overline{\phi}(0) = \hat{y} = (\alpha)\exp(x\beta) \cdot (e) \tag{10}$$

Equation (10) can be written in Equation (11).

$$\ln(\hat{y}) = \ln(\alpha) + x\beta + \ln(e) \tag{11}$$

Based on Equation (11), we can derive the higher order of $\hat{y}$ or $r_{NF}(0,0)$. The equation is shown in Equation (12).

$$\ln(\hat{y}) = \ln(\alpha) + (\beta_1)\ln(X) + (\beta_2)\ln\left(X^2\right) + \cdots + (\beta_M)\ln\left(X^M\right) + \ln(e) \tag{12}$$

Equation (12) can be simplified into Equation (13).

$$\hat{Y} = \alpha e \prod_{k=1}^{M} \left(X^k\right)^{\beta_k} \tag{13}$$

After the x and y axes values are determined, they are substituted into Equation (12). After the calculation is done, the α and β_M can be obtained. The order of Equation (13) is decided by the M. Then, α and β_M values are substituted into Equation (13) to get the estimated noise-free peak value $\hat{y}$ [9].

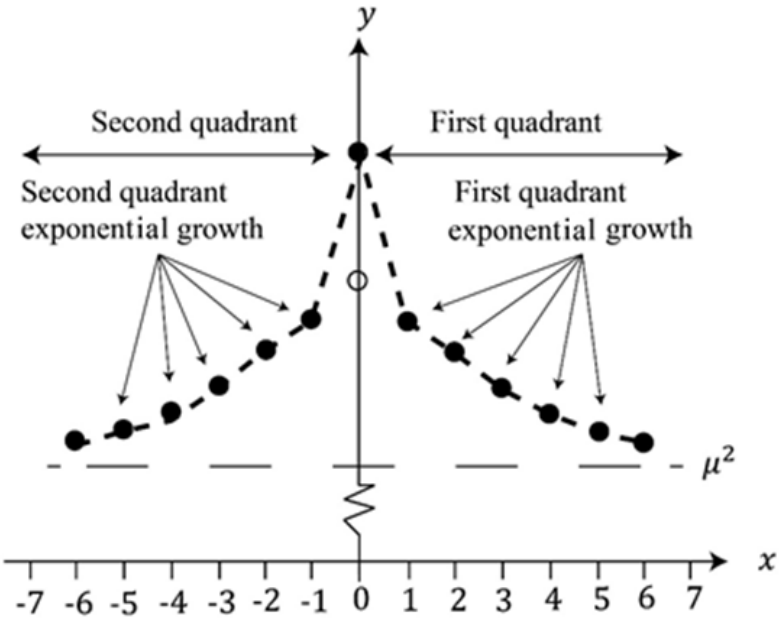

FIGURE 5. Exponential increment of an ACF curve

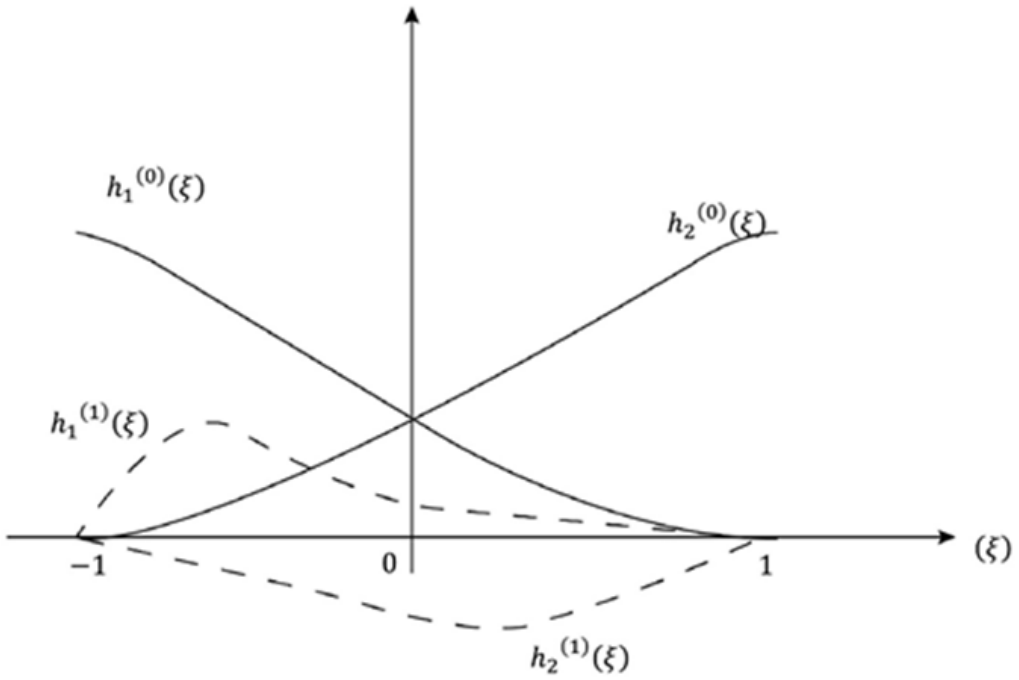

FIGURE 6. Four Hermite basic functions

3.4. **Adaptive tuning piecewise cubic hermite interpolation.** A mathematical model called piecewise cubic Hermite interpolating polynomial (PCHIP) was proposed in [26]. The theory behind the PCHIP function is that it is the combination of multiple sub-functions. Each sub-function is constructed using a cubic polynomial model. These functions make an interpolation between two known nodes and the derivatives at the nodes are known. PCHIP function can preserve the shape due to its smooth first derivative. Other than that, PCHIP function has no overshooting problem and less oscillation when compared to other models.

The PCHIP model is then defined as:

$$P(x) = \frac{3hs^2 - 2s^2}{h^3} y_{k+1} + \frac{h^3 - 3hs^2 + 2s^3}{h^3} y_k + \frac{s^2(s-h)}{h^2} d_{k+1} + \frac{s(s-h)^2}{h^2} d_k \tag{14}$$

where $s = x - x_i$ and $h = h_i$.

Lastly, Equation (14) is applied on $-1 \leq x \leq 0$ to calculating the noise-free zero offset point $\overline{r}_{11}(0,0)$ [24-26].

Based on PCHIP method, a multiplier M is introduced to achieve better performance, and called as adaptive tuning piecewise cubic Hermite interpolation (ATPCHIP). The ATPCHIP model is then defined as:

$$P(x) = \frac{3hs^2 - 2s^2}{h^3} y_{k+1} + \frac{h^3 - 3hs^2 + 2s^3}{h^3} y_k + M\left(\frac{s^2(s-h)}{h^2} d_{k+1} + \frac{s(s-h)^2}{h^2} d_k\right) \tag{15}$$

where $s = x - x_i$ and $h = h_i$.

In addition, ATPCHIP is presented as better-performed SNR estimation method for single image application.

4. **The Cramer-Rao Inequality and Statistical Tests for SNR Estimation Performance.** Four tests are used to test performance of the SNR estimation results, and they are Cramer-Rao inequality test and statistical tests. The statistical tests are t-test, scatter plot, and Bland-Altman plot.

4.1. **Statistical tests.**

4.1.1. *T-test.* For the performance of t-test using data analysis tool in Excel, we first assume that the mean of the two datasets is unknown. From each of the two datasets, the real noise-free peak value (NF) and the estimated noise-free peak value ($\hat{y}$) are found. The mean and variance of each set of data are then calculated. After that, the p-value, t-stat, and t-critical of two-tail test are determined. The p-value is the probability of getting a result equal to or higher than the actual situation if the null hypothesis is true. The confident or significant level α is set to be equal to 0.05. α is also the probability of wrongly rejecting the null hypothesis [27]. The null hypothesis (H_0) is set when the $\hat{y}$ is the same as NF.

There are two situations to justify the rejection of the null hypothesis. First, when the p-value is equal to or less than α. Second, when the t-stat does not fall between the negative t-critical and t-critical.

4.1.2. *Scatter plot.* Scatter plot or correlation chart is used to determine the correlation between two variables. It shows the similarity and relevance between two variables. The independent variable is set as the NF and the dependent variable is the $\hat{y}$. We can verify that the $\hat{y}$ is correlated with the real values, if the plot shows a line or a curve.

4.1.3. *Bland-Altman plot.* The Bland-Altman plot [31] is a method used to compare two clinical measurements. It is a new measurement compared with the golden standard. The first item that needs to be calculated is the mean difference of NF and $\hat{y}$. The second item is the 95% limits of agreement, which acts as the mean difference. This value is equal to $1.96 \times SD$, where SD is the standard deviation. This method presents graphically the difference of two data sets against the mean for each data in order to test whether the estimated data match with the real data. The two parameters needed are Equation (16) and Equation (17), where D is the mean of difference, and N is the number of samples.

$$\left(\overline{\hat{y} - x}\right) = D = \frac{\sum \hat{y} - NF}{N} \tag{16}$$

$$SD = \sqrt{\frac{\sum \left((\hat{y} - NF) - \left(\overline{\hat{y} - NF}\right)\right)^2}{N - 1}} \tag{17}$$

After the D and SD are calculated, two lines are drawn on the diagram, which are $D + 1.96 \times SD$, and $D - 1.96 \times SD$. The graph of $(\hat{y} - NF)$ versus $\frac{NF+\hat{y}}{2}$ is then plotted. If the majority of the points fall in the confident range, we can conclude that the y data (estimated values) is able to replace the x data (real value).

4.2. **Cramer-Rao lower bound.**

The Cramer-Rao lower bound (CRLB) is a method to get the lower bound of the data mean squared error (MSE). If the performance of the unbiased estimator is the same as or slightly higher than the CRLB, the estimator can be concluded as an efficient estimator. In this paper, CRLB is used to quantify the performance bounds for the estimator [14,31-34].

Given that an SEM image $g(x, y) = s(x, y) + w(x, y)$, where $g(x, y)$ is the noisy image, $s(x, y)$ is the noise-free image, and $w(x, y)$ is the additive Gaussian white noise

$$p(w) = p(x, \theta) = \frac{1}{\sqrt{2\pi\sigma}} e^{-\frac{(w-s)^2}{2\sigma^2}} \tag{18}$$

The SNR of single image is defined as in Equation (19).

$$SNR = (\theta_1, \theta_2) = \frac{S^2}{\sigma^2} \tag{19}$$

The estimated of α is based on the L observed pixels of $w(n)$, which is the resolution of the image. The estimator is dependent on two parameters, which are the signal S and the noise variance σ^2. Therefore, the θ in Equation (19) is defined as in Equation (20).

$$\theta = (\theta_1, \theta_2) = \left[S, \sigma^2\right] \tag{20}$$

The estimated SNR is commonly calculated in dB unit. Therefore, Equation (20) can be represented in Equation (21).

$$g(\theta) = SNR_{dB} = 10 \log \left(\frac{S^2}{\sigma^2}\right) \tag{21}$$

The CRLB function of the multi-parameter is shown in Equation (22)

$$CRLB(g(\theta)) = \frac{\partial g(\theta)}{\partial \theta} F^{-1} \frac{\partial g(\theta)^T}{\partial \theta} \tag{22}$$

where $F(\theta)$ indicates the Fisher information matrix, defined:

$$F(\theta) = \begin{bmatrix} -E\left(\dfrac{\partial^2 \ln p(x,\theta)}{\partial S^2}\right) & -E\left(\dfrac{\partial^2 \ln p(x,\theta)}{\partial S \partial \sigma^2}\right) \\ -E\left(\dfrac{\partial^2 \ln p(x,\theta)}{\partial (\sigma^2) \partial (S^2)}\right) & -E\left(\dfrac{\partial^2 \ln p(x,\theta)}{\partial (\sigma^2)^2}\right) \end{bmatrix} \tag{23}$$

where $p(x, \theta)$ indicates the pdf of additive Gaussian white noise and E indicates the expected value. The $\ln p(x, \theta)$ is

$$\ln p(x,\theta) = -\frac{1}{2}\ln(2\pi) - \frac{1}{2}\ln(\sigma^2) - \frac{1}{2\sigma^2}(w - S)^2 \tag{24}$$

The expected values in Fisher information matrix are calculated and shown in Equation (25) to Equation (28).

$$-E\left(\frac{\partial^2 \ln p(x,\theta)}{\partial S^2}\right) = E\left(\sigma^2\right) = \sigma^2 \tag{25}$$

$$-E\left(\frac{\partial^2 \ln p(x,\theta)}{\partial S \partial (\sigma^2)}\right) = -\sigma^4 E(w - S) = 0 \tag{26}$$

$$-E\left(\frac{\partial^2 \ln p(x,\theta)}{\partial (\sigma^2) \partial (S^2)}\right) = \sigma^4 E(w - S) = 0 \tag{27}$$

$$-E\left(\frac{\partial^2 \ln p(x,\theta)}{\partial (\sigma^2)^2}\right) = \frac{\sigma^4}{2} \tag{28}$$

Therefore, Equation (23) can be written as

$$F(\theta) = \begin{bmatrix} \dfrac{1}{\sigma^2} & 0 \\ 0 & \dfrac{1}{2\sigma^4} \end{bmatrix} \tag{29}$$

Since we have L observed pixels, Equation (29) is rewritten as

$$F(\theta) = L \begin{bmatrix} \dfrac{1}{\sigma^2} & 0 \\ 0 & \dfrac{1}{2\sigma^4} \end{bmatrix} \tag{30}$$

By applying the inverse matrix formula, $F^{-1}(\theta)$ is

$$F^{-1}(\theta) = \begin{bmatrix} \frac{\sigma^2}{L} & 0 \\ 0 & \frac{2\sigma^4}{L} \end{bmatrix} \tag{31}$$

Next, the derivative of $g(\theta)$ is calculated with respect to S and σ.

$$\frac{\partial g(\theta)}{\partial \theta} = \begin{bmatrix} \frac{\partial g(\theta)}{\partial S} & \frac{\partial g(\theta)}{\partial \sigma} \end{bmatrix} \tag{32}$$

$$\frac{\partial g(\theta)}{\partial \theta} = \begin{bmatrix} \frac{20}{\ln(10)S} & \frac{-10}{\ln(10)\sigma^2} \end{bmatrix} \tag{33}$$

Equation (32) and Equation (33) are substituted into Equation (22) and shown in Equation (34). Equation (34) is simplified into Equation (35).

$$CRLB(g(\theta)) = \frac{\partial g(\theta)}{\partial \theta} F^{-1} \frac{\partial g(\theta)^T}{\partial \theta} \tag{34}$$

$$CRLB(g(\theta)) = \frac{400}{L \ln(10)^2} \left(\frac{1}{SNR_{dB}} + \frac{1}{2} \right) \tag{35}$$

5. **Results.**

5.1. **Statistical test using ATPCHIP and other existing methods.**

The t-test, scatter plot and Bland-Altman plot are used to test the results. The 1240 samples of different noise variance between in the range of 0.001 to 0.01 are used for the data analysis.

5.1.1. *Performance of the ATPCHIP compared with existing methods using t-test.* Table 1 shows the mean and variance of the real value and the estimated value of ATPCHIP and other existing methods.

TABLE 1. Comparison of t-test two-sample results of ASNN, LLSR, NLLSR and ATPCHIP by assuming unequal variances

	ASNN		LLSR		NLLSR		ATPCHIP	
	Real	Estimated	Real	Estimated	Real	Estimated	Real	Estimated
Mean	0.214438	0.204963	0.214438	0.21574	0.214438	0.21276	0.214438	0.214495
Variance	0.005242	0.005162	0.005242	0.005203	0.005242	0.005154	0.005242	0.005240
Observations	1240	1240	1240	1240	1240	1240	1240	1240
Hypothesized Mean Difference	–	0	–	0	–	0	–	0
t-stat	–	1.39	–	0.4484	–	0.5793	–	0.01960
p-value	–	0.15	–	0.65	–	0.65	–	0.90
t-critical two-tail	–	1.960922	–	1.960922	–	1.96	–	1.960922
Mean Difference	0.009475		0.001302		0.001678		0.00005	
Variance Difference	0.00008		0.000039		0.000088		0.000001	

From Table 1, the p-values are larger than the confident level α. Therefore, we cannot reject the null hypothesis. The second criteria are shown as below:

1) t-stat = 0.016951 > – t-critical = – 1.960922

2) t-stat = 0.016951 < t-critical = 1.960923

Since the t-stat and t-critical values do not fulfil the criteria, we cannot reject the null hypothesis. We conclude from t-test that the null hypothesis cannot be rejected, as the estimated noise-free peak using ATPCHIP method is similar to the real noise-free peak.

According to Table 1, ATPCHIP is the lowest in mean difference and variance difference which indicated that it outperforms other methods by having the output values nearest to the real noise-free peak value. This indicates ATPCHIP method has better SNR estimation.

5.1.2. *Performance of the ATPCHIP compared with existing methods using scatter plot.* Figure 7 shows the scatter plots of estimated points versus the real points by using ASNN, LLSR, NLLSR and ATPCHIP.

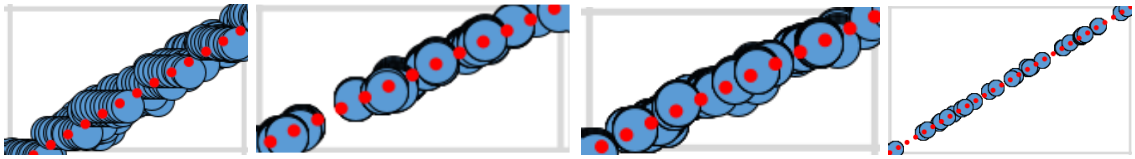

(a) (b) (c) (d)

FIGURE 7. Scatter plots of estimated values versus real values using: (a) ASNN, (b) LLSR, (c) NLLSR, and (d) ATPCHIP

Scatter plot is applied to verifying the similarity of the two datasets. It is obvious that the data form a line. In comparison, ATPCHIP estimated noise-free peak results as shown in Figure 7(d) are more consistent and nearer to the real noise-free peak. ATPCHIP utilized adaptive tuning onto the PCHIP model and achieved better SNR estimation.

5.1.3. *Performance of the ATPCHIP compared with existing methods using Bland-Altman plot.* For the Bland-Altman plot, D and SD are calculated. Therefore, the confident range is between $D + 1.96 \times SD$ and $D - 1.96 \times SD$.

Figure 8 shows the Bland-Altman plot of the real and the estimated peak for ASNN, LLSR, NLLSR and ATPCHIP respectively. For ASNN and NLLSR, it can be observed in Figures 8(a) and 8(c) that the majority of the points are falling within the confident range. We can conclude that the estimation values can replace the real value. Figure 8(b) shows the poor performance of LLSR as majority point fell outside the confident range. This shows that a lot of LLSR output values are in error.

From Figure 8(d), we observe that almost all the output points of ATPCHIP are within the confident range. Therefore, it can be concluded that the ATPCHIP outperforms the other methods and its results can replace the real-noise-free peak value. ATPCHIP implements adaptive tuning properties to PCHIP model and is capable of generating the output point with confident range.

Concluded from the conducted t-test, scatter diagram and Bland-Altman diagram of the three proposed methods, the ATPCHIP shows best results, as it has the least mean difference with the real value. Besides, in the Bland-Altman diagram, almost all the output points are within the confident range. Henceforth, the ATPCHIP method is preferred against other compared methods.

5.2. **Performance of the ATPCHIP compared with existing methods using Cramer-Rao lower bound.** As a performance of the ATPCHIP model, the noise variance is estimated. We take four kinds of SEM noise-free images with size 256×256 pixels, namely, images of wood fibre composite material, silver paint, IC wire bonding, and solder

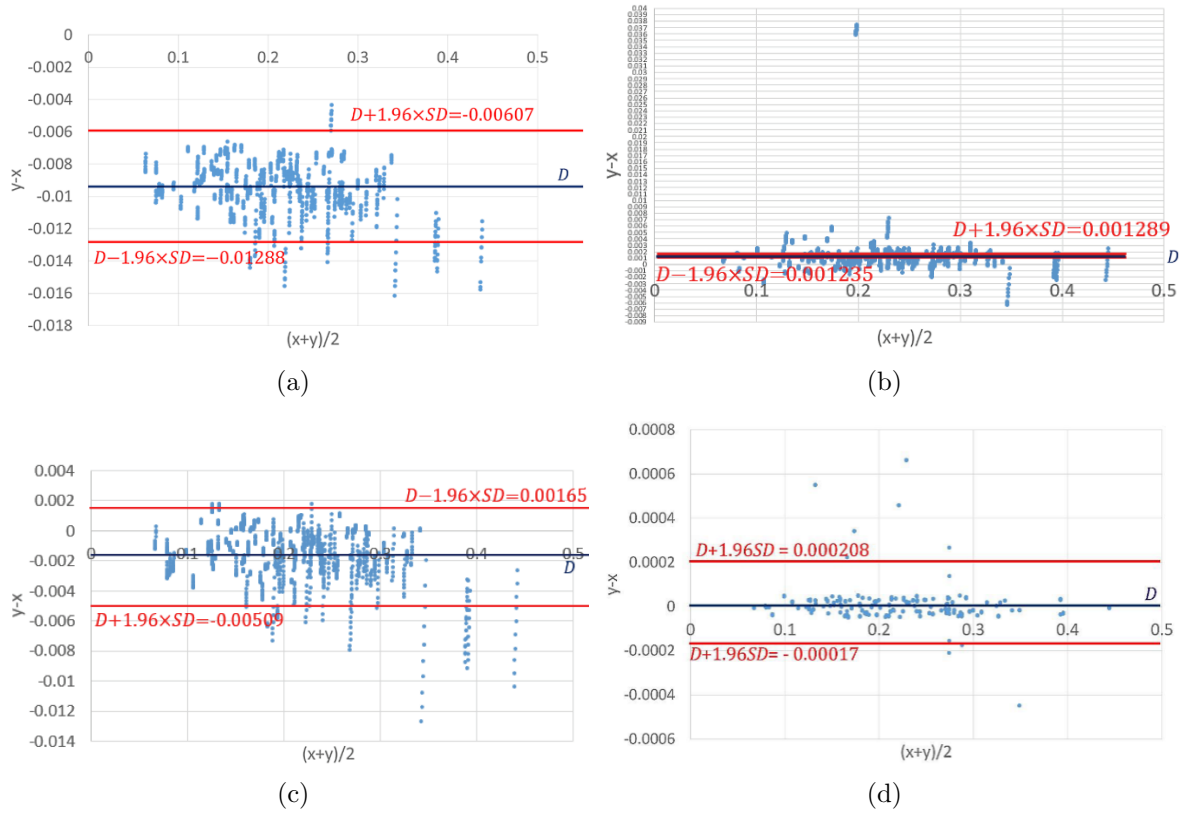

FIGURE 8. Bland-Altman plot of: (a) ASNN, (b) LLSR, (c) NLLSR, and (d) ATPCHIP

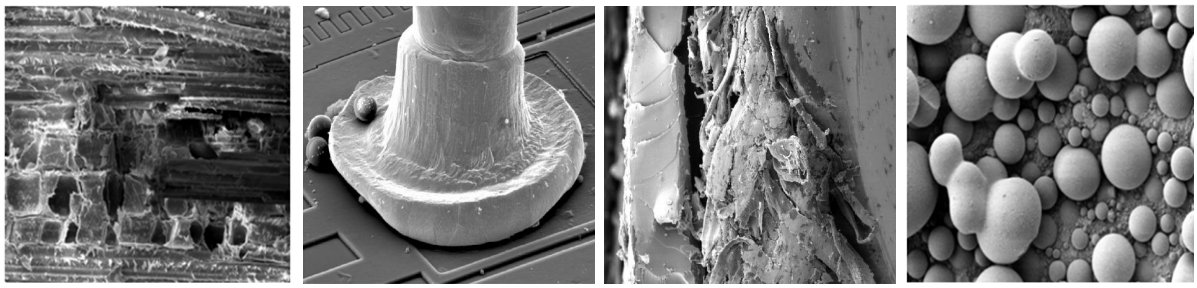

FIGURE 9. Four selected images to test the performance of the ATPCHIP method: (a) wood fiber composite material; (b) silver paint; (c) IC wire bonding; (d) sample images of power IC captured at beam diameter = 151nm

bolding as in Figure 9. White noise is augmented into the images, and the autocorrelation functions are then computed.

As a single indication of error, the square root of the MSE matrix trace for each estimator and the bound of Equation (36) and Equation (37) are computed. The square root of the trace of the MSE matrix gives a valid computation of the mean magnitude bounds as for the CRLB, as shown in Tables 4 and 7.

Figures 10, 11, 12, and 13 show the performance of the various methods as a function of SNR. The MSE shown in the tables has been normalized using Equation (36) and

Equation (37).

$$\widetilde{MSE} = MSE/(SNR_{actual}) \tag{36}$$

$$\widetilde{CRLB} = CRLB/(SNR_{actual}), \tag{37}$$

where $\widetilde{MSE}$ is the mean square error after normalization and $\widetilde{CRLB}$ is the Cramer-Rao lower bound after normalization.

Figure 9 shows the four images selected randomly from database. These images are used to represent the performance of the ATPCHIP method by comparing with ASNN, LLSR and NLLSR. There are images with noise variance (NV) of 0.001 to 0.01 for each image as shown in Figure 9. The SNR in dB is calculated and the mean square error (MSE) is calculated by comparing with the noise-free (NF) image. Table 2 shows the SNR in dB using various methods.

From Table 2, we can observe that the ATPCHIP method has the closest estimated SNR by comparing with NF in different noise variances. For NLLSR, the estimated value has larger difference when NV is smaller. ASNN method has similar estimation results compared to NLLSR. LLSR shows least accurate among the four methods. The performance of each method can be seen clearly if the results are represented using MSE. The results of Table 2 in terms of MSE are shown graphically in Figure 10.

From Figure 10, the ASNN has the highest MSE. This means that the difference between ASNN and the NF is the highest. Hence, the estimation results are not satisfactory. The second highest MSE is the NLLSR. Although NLLSR gives better estimation compared to ASNN, the MSE is still very high. LLSR has lower MSE compared to NLLSR and ASNN. ATPCHIP shows better results compared to the other three existing methods. The MSE values of ATPCHIP are the lowest among all methods. As the NV is higher, the ATPCHIP gives better estimation and has lower MSE value.

Figure 10 shows that the performance of ATPCHIP for wood fiber composite material with horizontal field width of 50μm is better than other methods. For the SNR range from 0.001 to 0.01, the error variance of ATPCHIP is about 1% different from the CRLB. For the noise variance from 0.001 to 0.01, the other methods, except ATPCHIP, have the MSE deviating further from CRLB. The ATPCHIP can predict accurately the zero-offset point at low noise.

From Table 3, the ASNN shows the lowest estimated SNR values. It has large differences compared to the NF. For NV = 0.001, ASNN estimated SNR is 11.37dB, but the actual

Table 2. Comparison of calculated SNR of NF, ASNN, LLSR, NLLSR and ATPCHIP, using Figure 9(a)

	SNR (dB)				
Noise variance	NF	ASNN	LLSR	NLLSR	ATPCHIP
0.001	34.75	19.62	20.55	22.95	34.75
0.002	28.63	17.82	20.79	18.66	28.64
0.003	25.17	16.24	19.94	17.47	25.18
0.004	22.07	15.20	18.33	16.02	22.08
0.005	20.19	14.13	17.08	14.90	20.18
0.006	18.47	13.24	15.34	13.57	18.47
0.007	17.54	12.33	14.37	12.62	17.55
0.008	16.29	11.68	13.60	11.91	16.29
0.009	15.06	11.02	12.80	11.14	15.09
0.010	13.96	10.35	12.52	10.61	13.96

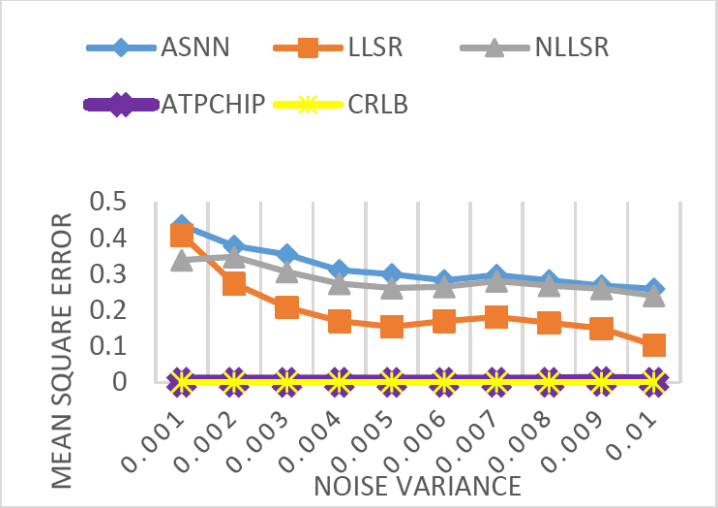

FIGURE 10. The comparison of mean square errors for various methods on wood fiber composite material image

SNR of that particular image is 41.04dB. LLSR has better SNR estimation compared to ASNN. However, the difference between the LLSR and the NF is still large. For the NLLSR, the SNR is higher than ASNN. When NV = 0.001, the accuracy of the NLLSR is better than LLSR. However, the overall result of LLSR is better than the NLLSR. ATPCHIP shows better estimation compared to ASNN, LLSR and NLLSR. The estimated SNR using ATPCHIP is slightly higher than NLLSR. The MSE of each method is calculated by comparing to the real NF SNR, and the results are shown in Table 4 and Figure 11.

From Figure 11, we can clearly see that the method with the highest MSE is the LLSR. By comparing to LLSR and ASNN, the MSE of the NLLSR and the ATPCHIP are low. However, ATPCHIP gives lower MSE as compared to NLLSR.

Figure 11 compares the performance of the various methods for the silver paint sample with horizontal field width of 100μm. The error variance of ATPCHIP algorithm is about 0.1%, close to that of the CRLB. The other methods are considerably less accurate, with error variance further away.

TABLE 3. Comparison of calculated SNR of NF, ASNN, LLSR, NLLSR and ATPCHIP, using Figure 9(b)

	SNR (dB)				
Noise variance	NF	ASNN	LLSR	NLLSR	ATPCHIP
0.001	41.04	11.37	31.78	32.82	40.66
0.002	31.71	10.40	26.60	26.65	31.88
0.003	27.51	9.54	23.33	23.11	28.44
0.004	24.48	8.73	21.00	20.53	24.00
0.005	22.64	8.00	19.15	18.53	22.82
0.006	20.58	7.41	17.64	16.88	20.77
0.007	19.67	6.69	16.37	15.61	19.09
0.008	17.88	6.22	15.14	14.39	17.70
0.009	16.87	5.61	14.16	13.36	16.75
0.010	15.67	5.02	13.29	12.40	15.85

TABLE 4. Comparison of calculated mean squared error results with Cramer-Rao lower bound for Figure 9(b)

Noise variance	ASNN	LLSR	NLLSR	ATPCHIP	CRLB
0.001	0.412537	0.7229	0.2256	0.0093	0.000152745
0.002	0.355146	0.6720	0.1611	0.0054	0.000154646
0.003	0.326055	0.6530	0.1520	0.0340	0.000156187
0.004	0.30599	0.6434	0.1421	0.0196	0.000157654
0.005	0.298438	0.6465	0.1540	0.0081	0.000158992
0.006	0.279181	0.6400	0.1427	0.0094	0.000160534
0.007	0.286779	0.6598	0.1677	0.0293	0.000161667
0.008	0.287176	0.6519	0.1530	0.0099	0.000162814
0.009	0.265192	0.6671	0.1604	0.0068	0.000164574
0.01	0.272012	0.6796	0.1519	0.0115	0.000165835

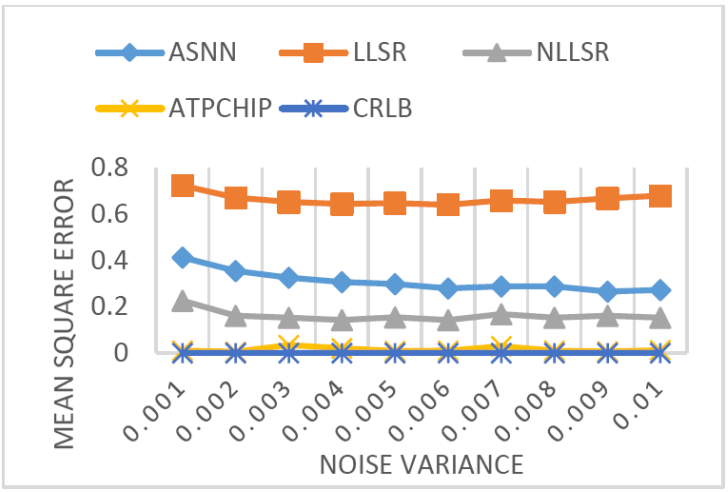

FIGURE 11. The comparison of mean square error versus noise variance for silver paint material

From the results in Table 5, ATPCHIP has the highest estimated SNR values. The second highest estimated SNR is the LLSR method. In this table, LLSR has better performance compared to ASNN. However, the differences between the estimated SNR values and the real NF values are higher. The MSEs are calculated and shown in Figure 12 graphically.

From Figure 12, we can clearly see that the ASNN has the highest MSE when compared to the other three methods. NLLSR has lower MSE than ASNN but is slightly higher than the LLSR. Among the four estimation methods, ATPCHIP shows the best performance.

From Table 6, the LLSR and NLLSR methods show similar results. Both LLSR and NLLSR give poorer estimation as compared to ATPCHIP. For NV = 0.001, the estimated SNR using ASNN is only 42.53dB, when the real value is 48.78dB. NLLSR has slightly better performance compared to LLSR. The estimated SNR using ATPCHIP is better than NLLSR and the result is closer to the real NF SNR. Therefore, it has the best estimation. The MSEs of the four estimation methods are shown in Table 7.

The ASNN has the highest MSE among the four methods, as shown in Table 7 and Figure 13. The MSE of LLSR is closed to NLLSR when NV = 0.006. ATPCHIP has the lowest MSE among the four methods. The tabulated results showed that ATPCHIP

TABLE 5. Comparison of calculated SNR of NF, ASNN, LLSR, NLLSR and ATPCHIP, using Figure 9(c)

	SNR (dB)				
Noise variance	NF	ASNN	LLSR	NLLSR	ATPCHIP
0.001	42.63	12.55	32.88	31.97	42.91
0.002	34.59	11.74	28.31	27.33	35.24
0.003	30.92	11.04	25.27	24.33	30.16
0.004	27.05	10.44	23.16	22.25	27.41
0.005	25.53	9.74	21.36	20.41	24.96
0.006	23.77	9.23	19.93	18.94	23.85
0.007	22.43	8.63	18.69	17.68	22.04
0.008	20.80	8.09	17.63	16.59	20.90
0.009	19.61	7.67	16.67	15.61	19.49
0.010	18.61	7.20	15.83	14.74	18.74

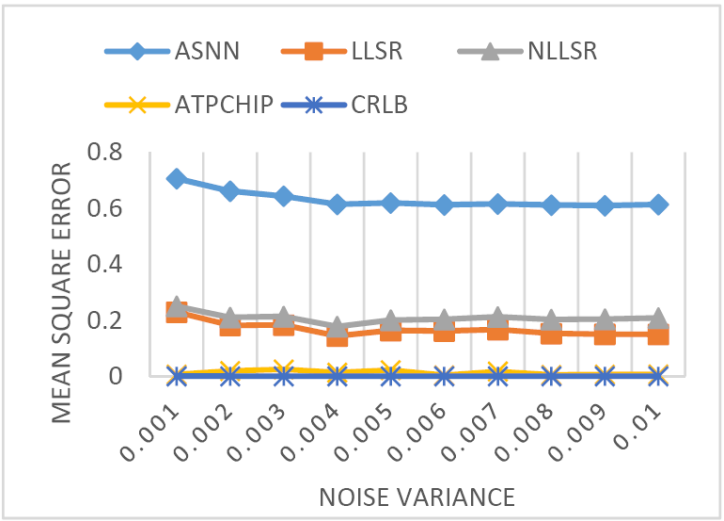

FIGURE 12. The comparison of mean square error versus noise variance for Figure 9(c)

TABLE 6. Comparison of calculated SNR of NF, ASNN, LLSR, NLLSR and ATPCHIP, using Figure 9(d)

	SNR (dB)				
Noise variance	NF	ASNN	LLSR	NLLSR	ATPCHIP
0.001	48.78	42.53	34.94	39.95	49.75
0.002	39.64	34.14	29.33	30.96	38.91
0.003	32.30	28.56	25.87	26.59	31.73
0.004	28.96	25.01	23.47	23.80	30.29
0.005	26.36	23.12	21.62	21.68	27.02
0.006	24.85	20.62	20.02	19.86	24.34
0.007	22.93	19.14	18.70	18.42	22.46
0.008	21.68	17.83	17.56	17.19	21.48
0.009	20.14	16.42	16.60	16.17	19.63
0.010	19.32	15.59	15.71	15.19	18.91

TABLE 7. Comparison of calculated mean squared error results with Cramer-Rao lower bound for sample images of power IC captured at beam diameter 151nm from Figure 9(d), with a horizontal field width of 100μm

Noise variance	ASNN	LLSR	NLLSR	ATPCHIP	CRLB
0.001	0.1282	0.2837	0.6886	0.0198	0.000152
0.002	0.1388	0.2601	0.2190	0.0184	0.000153
0.003	0.1158	0.1991	0.1768	0.0178	0.000154
0.004	0.1365	0.1896	0.1782	0.0458	0.000155
0.005	0.1230	0.1798	0.1775	0.0250	0.000156
0.006	0.1704	0.1944	0.2008	0.0204	0.000157
0.007	0.1653	0.1845	0.1967	0.0206	0.000157
0.008	0.1774	0.1900	0.2071	0.0094	0.000158
0.009	0.1847	0.1758	0.1971	0.0251	0.000159
0.01	1.0000	0.1869	0.2138	0.0214	0.00016

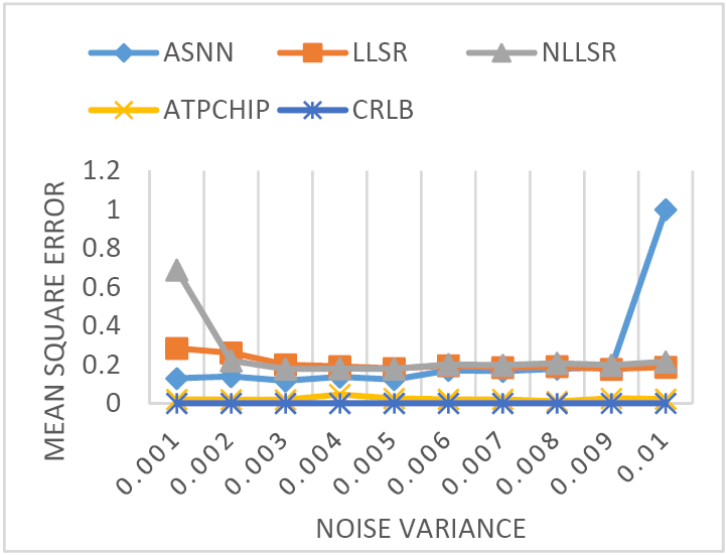

FIGURE 13. The comparison of mean square error versus noise variance for sample images of power IC captured at beam diameter 151nm

performed well on all experimental setup and proved its potential for other applications, for example, application on medical images [36-39].

6. **Concluding Remark.** An SNR estimation algorithm, ATPCHIP, has been proposed to recover the variance of additively corrupted zero mean noise. The method estimates SNR through a single image. The added noise is considered white, and details in the image are correlated over distances of at least a few pixels. The ATPCHIP needs a moderate amount of computation and in return can give the needed accuracy and independence. Consequently, the proposed methodology has potentials in real-time imaging system.

REFERENCES

[1] J. Li, F. Wang and D. Jiang, DOA estimation based on real-valued cross correlation matrix of coprime arrays, *Sensors*, vol.17, no.3, 2017.

[2] S. J. Erasmus, Reduction of noise in TV rate electron microscope images by digital filtering, *Journal of Microscopy*, vol.127, pp.29-37, 1982.

[3] D. C. Joy, SMART – A program to measure SEM resolution and imaging performance, *Journal of Microscopy*, vol.208, pp.24-34, 2002.
[4] J. Sijbers, P. Scheunders, N. Bonnet, D. D. Van and E. Raman, Quantification and improvement of signal-to-noise ratio in a magnetic resonance image acquisition procedure, *Magnetic Resonance Imaging*, vol.14, pp.1157-1163, 1996.
[5] J. T. Thong, K. S. Sim and J. C. Phang, Single-image signal-to-noise ratio estimation, *Scanning*, vol.23, pp.328-336, 2001.
[6] K. S. Sim and N. S. Kamel, Image signal-to-noise ratio estimation using the autoregressive model, *Scanning*, vol.26, no.3, pp.135-139, 2004.
[7] K. S. Sim and V. Teh, Image signal-to-noise ratio estimation using adaptive slope nearest-neighborhood model, *Journal of Microscopy*, vol.260, pp.352-362, 2015.
[8] K. S. Sim and S. NorHisham, Autoregressive linear least square single scanning electron microscope image signal-to-noise ratio estimation, *Scanning*, vol.38, no.6, pp.771-782, 2016.
[9] K. S. Sim and S. NorHisham, Nonlinear least squares regression for single image scanning electron microscope signal-to-noise ratio estimation, *Journal of Microscopy*, vol.264, no.2, pp.159-174, 2016.
[10] C. G. Shi, S. Salous, F. Wang and J. J. Zhou, Cramer-Rao lower bound evaluation for linear frequency modulation based active radar networks operating in a rice fading environment, *Sensors*, vol.16, p.2072, 2016.
[11] C. Shi, F. Wang and J. Zhou, Cramer-Rao bound analysis for joint target position and velocity estimation in FM-based passive radar networks, *IET Signal Processing*, vol.10, no.7, pp.780-790, 2016.
[12] H. Godrich, A. M. Haimovich and R. S. Blum, Target localization accuracy gain in MIMO radar-based systems, *IEEE Trans. Inf. Theory*, vol.56, pp.2783-2803, 2010.
[13] Q. He and R. S. Blum, The significant gains from optimally processed multiple signals of opportunity and multiple receive stations in passive radar, *IEEE Signal Processing Letter*, vol.21, pp.180-184, 2014.
[14] S. M. Kay, Cramer-Rao lower bound, in *Fundamentals of Statistical Signal Processing I: Estimation Theory*, NJ, Prentice Hall, 1993.
[15] B. M. Hamschin and M. T. Grabbe, An approximate Cramer-Rao lower bound for multiple LFMCW signals, *IEEE Trans. Aerospace and Electronic Systems*, vol.53, no.3, pp.1365-1374, 2017.
[16] J. Driggs, T. Sibbett, H. Moradiy and B. Farhang-Boroujeny, Channel estimation for filter bank multicarrier systems in low SNR environments, *IEEE International Conference on Communications (ICC-2017)*, 2017.
[17] J. J. Miller, L. Cochlin, K. Clarke and D. J. Tyler, Weighted averaging in spectroscopic studies improves statistical power, *Magnetic Resonance in Medicine*, vol.78, no.6, pp.2082-2094, 2017.
[18] D. R. Pauluzzi and C. Beaulieu, A comparison of SNR estimation techniques for the AWGN channel, *IEEE Trans. Communications*, vol.48, no.10, pp.1681-1691, 2000.
[19] T. Ertas and E. Dilaveroglu, Low-SNR asymptote of CRB and SNR estimates for BPSK in Nakagamim fading channels with diversity combining, *Electronics Letters*, vol.39, no.23, pp.1680-1682, 2003.
[20] D. Robinson and P. Milanfar, Fundamental performance limits in image registration, *IEEE Trans. Image Processing*, vol.13, no.9, pp.1185-1199, 2004.
[21] A. Filip and D. Shutin, Cramer-Rao bounds for L-band digital aeronautical communication system type 1 based passive multiple-input multiple-output radar, *IET Radar, Sonar & Navigation*, vol.10, no.2, pp.348-358, 2016.
[22] M. N. Javed, S. Ali and S. A. Hassan, 3D MCRLB evaluation of a UMTS-based passive multi-static radar operating in a line-of-sight environment, *IEEE Transaction of Signal Processing*, vol.64, pp.5131-5144, 2016.
[23] K. S. Sim, *Signal-to-Noise Ratio Estimation in Scanning Electron Microscope Imaging System*, Master Thesis, National University of Singapore, Singapore, 2002.
[24] H. L. Harter, *Least Squares: Encyclopedia of Statistical Sciences*, S. Kotz and N. L. Johnson (eds.), John Wiley & Sons, New York, 1983.
[25] A. Schneider, G. Hommel and M. Blettner, Linear regression analysis: Part 14 of a series on evaluation of scientific publications, *Deutsches Ärzteblatt International*, vol.107, no.44, pp.776-782, 2010.
[26] F. N. Fritsch and R. E. Carlson, Monotone piecewise cubic interpolation, *SIAM Journal Numerical Analysis*, vol.17, no.2, pp.238-246, 1980.
[27] A. Peirce, A Hermite cubic collocation scheme for plane strain hydraulic fractures, *Computer Methods in Applied Mechanics and Engineering (CMA)*, vol.199, no.29, pp.1949-1962, 2010.

[28] I. Iwashita, *Piecewise Polynomial Interpolations*, http://www.opengamma.com/sites/default/files/piecewise-polynomial-interpolation-opengamma.pdf, 2015.
[29] K. S. Sim, M. Y. Wee and W. K. Lim, Image signal-to-noise ratio estimation using shape-preserving piecewise cubic Hermite autoregressive moving average model, *Microscopy Research and Technique*, vol.71, pp.710-720, 2008.
[30] M. Paret, *Aphas, P-Values, and Confidence Intervals, Oh My!*, http://blog.minitab.com/blog/michelle-paret/alphas-p-values-confidence-intervals-oh-my, 2017.
[31] J. M. Bland and D. G. Altman, Statistical methods for assessing agreement, *Journal of Lancet*, vol.1, pp.307-310, 1986.
[32] K. S. Sim, M. E. Nia, C. P. Tso and W. K. Lim, Performance of new signal-to-noise ratio estimation for SEM images based on single image noise cross-correlation, *Journal of Microscopy*, vol.248, pp.120-128, 2012.
[33] K. S. Sim, H. T. Chuah and Z. Cheng, Robust image signal-to-noise ratio estimation using mixed Lagrange time delay estimation autoregressive model, *Scanning*, vol.26, no.6, pp.287-295, 2004.
[34] N. S. Alagha, Cramer-Rao bounds of SNR estimates for BPSK and QPSK modulated signals, *IEEE Communications Letter*, vol.5, no.1, pp.10-12, 2001.
[35] N. S. Kamel and K. S. Sim, Image signal-to-noise ratio and noise variance estimation using autoregressive model, *Scanning*, vol.26, pp.277-281, 2004.
[36] K. S. Sim, V. Teh and C. K. Lim, Local dynamic range compensation for scanning electron microscope imaging system by average mid-point local recursive mean separate histogram equalization, *International Conference on Robotics, Automation and Sciences (ICORAS)*, Melaka, 2016.
[37] F. F. Ting, K. S. Sim and E. K. Wong, A rapid medical image noise variance estimation method, *International Conference on Robotics, Automation and Sciences (ICORAS)*, Melaka, 2016.
[38] V. Teh, K. S. Sim and E. K. Wong, Extreme-level eliminating brightness preserving bi-histogram equalization technique for brain ischemic detection, *Proc. of the International Conference on Image Processing, Computer Vision, and Pattern Recognition (IPCV)*, pp.69-75, 2016.
[39] K. S. Sim, Z. X. Yeap and C. P. Tso, Signal-to-noise ratio estimation using adaptive tuning on the piecewise cubic Hermite interpolation model for images, *Scanning*, vol.38, pp.502-514, 2016.